RSC Advances

ROYAL SOCIETY OF CHEMISTRY

www.rsc.org/advances

Table of Content (TOC)

Comparative EPR Studies of Cu (II)-conjugated Phosphorous-Dendrimers in the Absence and Presence of Normal and Cancer Cells

M F. Ottaviani, N. E. Brahmi, M. Cangiotti, C. Coppola, F. Buccella, T. Cresteil, S. Mignani, A. M. Caminade, J. P. Costes, and J. P. Majoral

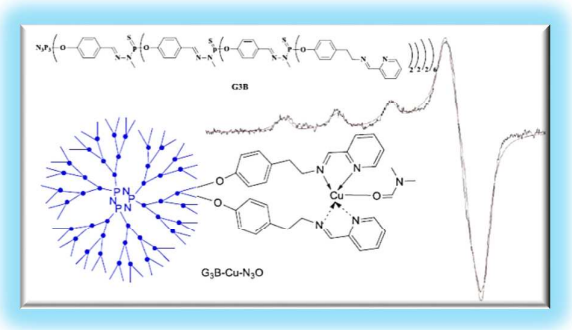

EPR analysis revealed peculiar structural and dynamical properties of anticancer-active **G3B**-Cu(II) in absence and presence of normal and cancer cells.

RSC Advances

RSCPublishing

ARTICLE

Comparative EPR Studies of Cu (II)-conjugated Phosphorous-Dendrimers in the Absence and Presence of Normal and Cancer Cells

Cite this: DOI: 10.1039/x0xx00000x

Received 00th January 2012,
Accepted 00th January 2012

DOI: 10.1039/x0xx00000x

www.rsc.org/

M F. Ottaviani,*[a] N. El Brahmi,[b,c] M. Cangiotti,[a] C. Coppola,[a] F. Buccella,[a] T. Cresteil,[d] S. Mignani,[e] A. M. Caminade,[b] J. P. Costes,[b] and J. P. Majoral*[b]

Comparative electron paramagnetic resonance (EPR) studies of both Cu (II)-conjugated phosphorous-dendrimers and the corresponding Cu (II)-monomers bearing different ligand moieties are presented, showing that the coordination mode, the chemical structure, the flexibility and the stability of these complexes are strongly depending on different parameters as the nature of the ligands, the size (generation) of the dendrimer, and the molar ratio between Cu (II) and the ligands. Studies are performed in the presence of HCT-116 cancer cells, and MRC-5 normal cells allowing to clarify the interaction mode of Cu (II) ions in a biological medium at different equilibration times. These studies point out the particular behavior of the Cu (II)-conjugated phosphorous-dendrimer at generation 3, decorated with *N*-(di(pyridine-2-yl)methylene)ethanamine moiety (termed **G3B)** The **G3B**-Cu (II) complex shows strong anticancer activity. The EPR analysis helped to clarify the unusual properties of this complex in the absence and presence of normal and cancer cells.

Introduction

Over the last decade, numerous nanomaterial systems and nanodevices have been developed as powerful strategies to deliver, for instance, drugs, vaccines, aptamers, siRNA, recombinant proteins and genes. Thus, the use of dendrimers in nanomedicine has rapidly grown in recent years and was reported in an increasing number of publications including several major reviews.[1] Recently, based on the huge therapeutic applications of biocompatible dendrimers, both active *per se* or as nano-carriers, we defined the dendrimer space concept as a new druggable sub-area which should enhance the druggability of specific target space such as kinases, and protein-protein interactions.[2]

The increase in the number of publications and interest can be explained by many featured major advantages of dendrimers as drug carrier candidates based on their unique and tunable properties: i) dendrimers have: i) a well-defined globular structure, predictable molecular weight and monodispersity, thus favouring reproducible pharmacokinetics, ii) their size which is generation dependent can fit various biomedical purposes, iii) their lack of immunogenicity allows much safer choices *versus* synthesized peptide carriers, natural protein carriers, iv) their high penetration abilities through the cell membranes allows high cellular uptake level, v) due to the enhanced penetration and retention effect they lead to the preferential uptake of materials by cancers and inflamed tissues, vi) they can be used for a variety of routes of administration including non-classical routes as trans-dermal diffusion, trans-nasal diffusion and ocular delivery, vii) their size, shape, surface properties, influence, pharmacodynamic and pharmacokinetic (PK/PD) behaviors, etc.

The possibility to use dendrimers active *per se* was well documented[3] and significantly increases the chance to fight against many diseases as cancers and neurodegenerative diseases. The widespread success of cisplatin and derivatives in clinical treatment of various types of cancers has placed coordination chemistry of metal-drugs in pole position to tackle cancer progression. In this direction, the properties and more specially the antitumoral properties of dendrimer-conjugated metallodrugs for nanotherapy in oncology are not so intensively reported. Today, Pt and Ru metallodendrimers are the most representative examples of potential anticancer therapeutic agents.[4,5] In addition to these two metals, copper (I/II) complexes represent very interesting alternative anticancer strategies.[5] In spite of the fact that many copper complexes obtained from S-donor (thiosemicarbazones, thiosemicarbazides, dithiocarbamates, dithiolates...), O-donor (pyrazole, imidazole, indoles...), Schiff bases, polydendates, or P donor phosphine systems to name as a few, have been proposed as promising cytotoxic agents on the base of *in vitro*

assays, most of them consists on the complexation of Cu (II) and more scarcely Cu (I) with small ligands.[5] Surprisingly there are very few examples reporting the formation and the antitumoral properties of Cu (II) conjugated dendrimers. Indeed, a PAMAM based heptanuclear copper (II) metallodendrimer exhibits a strong *in vitro* cytotoxicity against leukemia (MOLT-4) and breast cancer MCF-7cell lines.[6]

Recently, we developed original multivalent Cu (II)-conjugated phosphorus biocompatible dendrimers showing potent antitumor activities.[7] These dendrimers have cyclotriphosphazene ring as core. The data suggested that cytotoxicity increased with the number of terminal moieties available and was boosted by the presence of complexed Cu (II) ions. The most potent antiproliferative effects have been obtained with the *N*-(di(pyridine-2-yl)methylene)ethanamine moiety (termed B) – as host-guest complexation chelator - on the surface of the generation 3 of phosphorous dendrimers bearing 48 ligand groups (Figure 1). Two other chelators have been studied: *N*-(di(pyridine-2-yl)methylene)ethanamine (termed C: Figure 1) and 2-(2-methylenehydrazinyl)-pyridine (termed A: Figure 1). The antiproliferative effects of Cu (II) phosphorus dendrimers against both solid and liquid tumor cell lines and the first structure activity relationships of cell growth inhibition against several cancer cell lines[7] prompted us to characterize more deeply such phosphorus dendritic complexes. For this purpose, electron paramagnetic resonance (EPR) studies of a variety of these phosphorus Cu (II) dendritic complexes were investigated in the present study and compared to that of the corresponding "monomeric" Cu (II) complexes. The computer aided analysis of the EPR spectra of Cu (II) complexing different dendrimers has also revealed to be a useful tool for characterizing dendrimer structure, interacting ability, and flexibility.[8-13]

The purpose of this manuscript is therefore to characterize the phosphorous-containing dendrimers -Cu (II) complexes bearing the A, B and C chelators at three different generations (Figure 1) in order to get accurate information on the complexation modes and the structure and stability of these complexes as well as the evolution of the complexation with the Cu (II)/ terminal ligands molar ratio. Due to the peculiar anticancer properties of Cu (II) – **G3B** complex,[7] EPR characterization of this complex in the presence of HCT-116 cancer cells and MRC-5 normal cells was also performed. For a matter of comparison, we also analyzed the spectra of the A, B, and C molecules in the same experimental conditions as the dendrimers, by adding Cu^{2+} ions at increasing concentration.

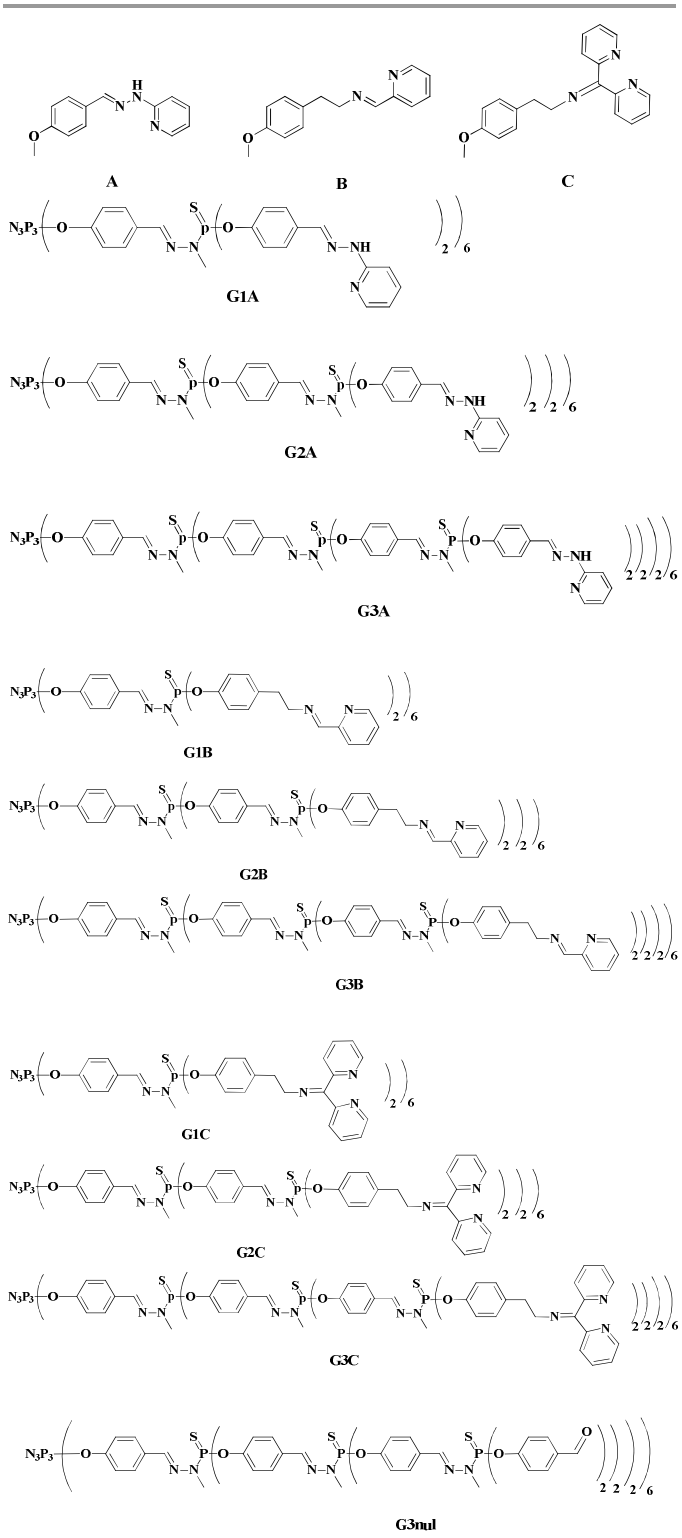

Figure 1: Structure of monomers and dendrimers of series A, B, C

Results and discussion

Cu (II)-dendrimers and monomers in the absence of cells

Figure 2 shows the EPR experimental spectra at 298 K of Cu (II) (0.1 M) solutions in DMF containing the dendrimers and the monomers at concentration of 0.1 M. For the dendrimers this concentration is related with the number of external surface

groups.The spectra were normalized at the same height. The different line shapes are due to the coexistence of different signals coming from different coordination sites and geometries. In most cases, two signals superimposed to each other in the spectra, whose main features were indicated with dashed lines in the figure. These signals were extracted by subtracting experimental spectra one from the other. Mainly, spectra showing only one component were subtracted from the spectra showing the same component superimposed to another one. Then, after calculating the relative percentages of the two components, we simulated both the signals.

Figure 2: EPR experimental spectra at 298 K of Cu (II) (0.1 M) solutions in DMF containing the dendrimers and the monomers at concentration of 0.1 M (for the dendrimers this concentration is in external surface groups). The spectra were normalized at the same height. The main peaks of the two components, corresponding to the coordination termed Cu-solvent and CuNxOy, were indicated with dashed lines in the figure.

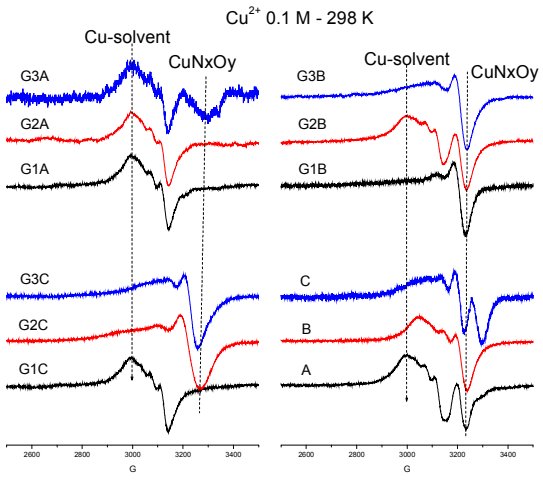

Several examples of computations of the EPR spectra and subtracted signals of Cu(II) at different concentrations, in DMF, in the presence of the various dendrimers, and at 298 and 150 K are reported in Figure S1 (Electronic Supplementary Information, ESI). The main parameters (components of the g tensor, component z of the A tensor, and correlation time for the rotational diffusion motion, τ) extracted from computation of key spectra are listed in Table 1. The meaning of these parameters is described in the Experimental Section. The different coordination types, listed in the last column of Table 1 were identified as described in the Experimental Section. The notation (CuNxOy) simply indicated how many oxygen (O) and/or nitrogen (N) sites were coordinating Cu^{2+} ions in a square planar geometry. For instance, a CuN2O2 coordination means that the Cu (II) ions coordinate 2 nitrogen and 2 oxygen sites.

Table 1: Main parameters (g_{ii}, A_{zz} and τ; meaning described in the Experimental Section) extracted from computation of key spectra (both at 298 and 150 K) at different Cu (II) concentrations and with monomers and dendrimers concentration of 0.1 M (in external surface groups for the dendrimers). The different coordination types, listed in the last column of the Table and obtained as described in the Experimental Section, indicated how many oxygen (O) and/or nitrogen (N) ligand sites were coordinating Cu2+ ions in a square planar geometry. In mixed coordinations, the oxygen sites come from the solvent molecules while nitrogen sites belong to the A, B and C groups. The accuracy is ±0.001 for g_{ii}, ± 0.5 G for A_{zz}, ± 0.01 ns for τ, and ± 2 % for the percentage

Cu^{2+} (M)	%	g_{xx}	g_{yy}	g_{zz}	A_{zz} (G)	τ (ns)	Coord.
A							
0.01	100	2.003	2.075	2.208	195	0.08	CuN4
0.05	100	2.018	2.05	2.23	165	0.08	CuN4
0.1	60	2.038	2.04	2.3	150	0.08	CuN2O2
--	40	2.06	2.07	2.385	121	0.05	Cu-solv
0.3	18	2.038	2.04	2.3	150	0.08	CuN2O2
--	82	2.06	2.07	2.385	121	0.05	Cu-solv
0.5	7	2.038	2.04	2.3	150	0.08	CuN2O2
--	93	2.06	2.07	2.385	121	0.05	Cu-solv
B							
0.01	100	2.03	2.064	2.256	160	0.07	CuN4-CuN3O
0.03	100	2.03	2.064	2.256	160	0.07	CuN4-CuN3O
0.1	85	2.031	2.065	2.26	155	0.07	CuN3O-CuN2O2
--	15	2.06	2.07	2.385	121	0.05	Cu-solv
0.3	30	2.031	2.065	2.26	155	0.07	CuN3O-CuN2O2
	70	2.06	2.07	2.385	121	0.05	Cu-solv
C							
0.01	100	2.016	2.052	2.233	165	0.3	CuN4
0.03	100	2.016	2.052	2.233	165	0.3	CuN4
0.05	100	2.016	2.052	2.233	165	0.3	CuN4
0.1	35	2.04	2.04	2.3	150	0.12	CuN2O2
--	65	2.006	2.048	2.221	178	0.4	CuN4
0.3	25	2.04	2.04	2.3	150	0.12	CuN2O2
--	75	2.06	2.07	2.385	121	0.05	Cu-solv
0.5	10	2.04	2.04	2.3	150	0.12	CuN2O2
--	90	2.06	2.07	2.385	121	0.05	Cu-solv
G1A							
0.01	100	--	--	--	--	--	
0.05	100	--	--	--	--	--	
0.1	100	2.06	2.07	2.385	121	0.05	Cu-solv
G2A							
0.01	100	2.008	2.05	2.22	170	3.3	CuN4
0.03	15	2.008	2.05	2.22	170	3.3	CuN4
--	85	2.06	2.07	2.385	121	0.05	Cu-solv
0.05	100	2.06	2.07	2.385	121	0.05	Cu-solv
0.1	100	2.06	2.07	2.385	121	0.05	Cu-solv
G3A							
0.01	100	2.021	2.06	2.255	160	7	CuN3O-CuN2O2
0.03	100	2.021	2.06	2.255	160	7	CuN3O-CuN2O2
0.1	50	2.032	2.07	2.272	145	4	CuN2O2-CuNO3
--	50	2.06	2.07	2.385	121	0.05	Cu-solv
0.3	100	2.06	2.07	2.385	121	0.05	Cu-solv
G1B							
0.01	100	2.03	2.064	2.256	160	1	CuN3O-CuN2O2
0.03	100	2.03	2.064	2.256	160	0.4	CuN3O-CuN2O2
0.05	100	2.03	2.064	2.256	160	0.2	CuN3O-CuN2O2
0.1	60	2.038	2.076	2.29	151	0.35	CuN2O2
	40	2.06	2.07	2.385	121	0.05	Cu-solv
G2B							
0.01							
0.03	100	2.038	2.05	2.288	163	0.33	CuN4-

							CuN3O
0.05	20	2.06	2.07	2.385	121	0.05	Cu-solv
--	80	2.038	2.05	2.288	163	0.33	CuN4-CuN3O
0.1	65	2.06	2.07	2.385	121	0.05	Cu-solv
--	35	2.038	2.05	2.288	163	0.33	CuN4-CuN3O
0.3	95	2.06	2.07	2.385	121	0.05	Cu-solv
--	5	2.038	2.05	2.288	163	0.33	CuN4-CuN3O
0.5	100	2.06	2.07	2.385	121	0.05	Cu-solv
G3B							
0.01	100	2.021	2.06	2.253	168	8	Cu-N4
0.03	100	2.021	2.06	2.255	160	7	CuN3O-CuN2O2
0.05	100	2.023	2.06	2.255	160	6	CuN3O-CuN2O2
0.1	100	2.04	2.048	2.298	152.5	0.23	CuN2O2
0.3	25	2.04	2.048	2.298	152.5	0.23	CuN2O2
--	75	2.06	2.07	2.385	121	0.05	Cu-solv
0.5	100	2.06	2.07	2.385	121	0.05	Cu-solv
G1C							CuN4-
0.01	100	2.018	2.05	2.23	165	2	CuN3O
0.03	100	2.03	2.04	2.28	150	4	CuN2O2
0.05	50	2.06	2.07	2.385	121	0.05	Cu-solv
--	50	2.04	2.04	2.3	150	0.17	CuN2O2
0.1	100	2.06	2.07	2.385	121	0.05	Cu-solv
G2C							CuN3O-
0.01	100	2.031	2.064	2.255	160	0.2	CuN2O2
0.05	100	2.031	2.064	2.255	160	0.2	CuN3O-CuN2O2
0.1	50	2.031	2.064	2.255	160	0.2	CuN3O-CuN2O2
	50	2.06	2.07	2.385	121	0.05	Cu-solv
G3C							
0.01							
0.05	100	2.023	2.06	2.255	160	6	CuN3O-CuN2O2
0.1	90	2.027	2.082	2.265	153	0.35	CuN2O2
--	10	2.06	2.07	2.385	121	0.05	Cu-solv
0.3	100	2.06	2.07	2.385	121	0.05	Cu-solv

The nitrogen sites in the dendrimers may belong to the external groups (A, B, C) and/or to the dendrimer internal backbone. On the other side, the oxygen sites may be solvent molecules or oxygen-containing groups of the dendrimer backbone. However, we noted that the EPR spectra of increasing Cu(II) concentrations in the presence of the dendrimers at generation 1, 2 or 3 bearing 12, 24 or 48 terminal aldehydes groups respectively (an example of this structure is shown in Figure 1: G3nul) , that is to say in the absence of the external functionalities A, B, and C, were the same as those found for the blanks (Cu(II) in DMF solutions). This means that the results listed in Table 1 and described in the following only came from Cu(II) complexed with the solvent molecules and/or with A, B, and C groups, both free in solution, or attached to the dendrimer structure. Complexation of Cu (II) with the oxygen and nitrogen sites within the cavities of the dendrimers (at the dendrimer internal backbone) is not occurring on the basis of the EPR results.

The first evidence in Table 1 is that, in all cases, after saturating the ligand and dendrimer coordination sites, at high Cu (II) concentrations the progressive increase of the Cu (II) – solvent complex masks the Cu (II) – ligand or Cu (II) - dendrimer complexes. However, to clarify the differences merging from the data listed in Table 1, we reported, in Figure 3, the histograms comparing selected main parameters, as follows:

Figures 3(A) and 3(B) show the variations of the g_{xx} and A_{zz} parameters, respectively, for the various systems. The g_{xx} parameter is the x component of the g tensor for the coupling between the unpaired electron spin and the magnetic field, while, the A_{zz} parameter is the z component of the A tensor for the coupling between the unpaired electron spin and the copper nuclear spin. These parameters well report about the progressive increase in oxygen coordination, that is, usually the higher g_{xx} and the lower A_{zz} indicate a higher number of oxygen ligands. Also, these parameters are affected by the geometry of the complex, that is, by eventual distortions of the square planar_structure. The comparison was performed at the same Cu (II) concentration (0.05 M). But, the comparison is complicated by the fact that sometimes the spectra are constituted by two components. This is the case for **G2B** and **G1C**: the spectra at Cu (II) concentration of 0.05 M were constituted by two components superimposing to each other at different relative percentages. One component is due to Cu-solvent complexation. By subtracting this component from the overall EPR spectra we extracted the second component at 80 % (for **G2B**) and 50 % (for **G1C**) relative percentages. This second component arises from Cu (II) complexed with the dendrimer ligands. The g_{xx} and A_{zz} values of this component are the ones reported in the histograms in Figure 3(A) and 3(B), respectively.

The analysis of these histograms indicates the following properties:

- Compared to A ligand, **G1A** and **G2A** dendrimers show a significant increase in the g_{xx} parameter, while A_{zz} significantly decreases. This indicates a loss of nitrogen binding sites for Cu (II) coordinating the A dendrimers with respect to the A ligand, which may be ascribed to the impediment played by the dendrimer branches for approaching the nitrogen ligands to Cu (II) at the correct geometry to form a chelate complex.
- The B ligand provides a higher g_{xx} value and a lower A_{zz} value with respect to A ligand and, more, to the C one. Therefore B is weaker complexing the Cu (II) ions than A and C in line with a more flexible ligand structure. **G1B** dendrimer shows similar interacting ability as B, since the g_{xx} and A_{zz} values are comparable to those of B. However, **G2B**, already at 0.05 M of Cu (II), shows a fraction (20 %) of free ions, and, for the interacting ions (80 %), both g_{xx} and A_{zz} values are higher than those for **G1B**. This indicates an anomalous behavior of **G2B** dendrimer, which may be ascribed to the density/distribution of nitrogen sites available for Cu (II) coordination which provides a more nitrogen-rich coordination, but also a more distorted geometry.
- **G1C** shows a similar, even worse behavior with respect to **G2B**, since 50 % of the ions (at concentration 0.05 M) are free (not bonded to the dendrimer). Furthermore, for the 50 % of bonded ions the increase in g_{xx} with the correspondent decrease in A_{zz} indicates less N sites binding

Cu (II) for this dendrimer with respect to the ligand. However, in the C case, the second generation dendrimer (**G2C**) behaves better that the first generation one (**G1C**) in respect to the interactions between the ions and the dendrimer nitrogen sites.

- In all cases, the G3 dendrimers show a lowering of the g_{xx} values and an increase in the A_{zz} values with respect to the G2 generations. This indicates an easier coordination with the dendrimer nitrogen sites, which is probably favored by the higher density of external functions for G3.

At the same 0.05 M concentration of Cu (II), it is also interesting to compare the correlation times for the rotational diffusion motion of the ions (τ, see the Experimental Section for more details) reported in Figure 3(C) for the various systems. This parameter reports about the strength of interaction between the ions and the ligands and is affected by the size of the ligands and the flexibility of the dendrimer branches containing the coordination sites. By analyzing this histogram we see that:

- The ligand C shows a higher τ value with respect to A and B, in agreement with both a bigger size of the C ligand, and a stronger bonding between the ligand and the ions, forming a chelate complex where two ligands coordinate one copper ion.
- The mobility decreases by increasing generation, in agreement with the increasing hindering of dendrimer branches flexibility and increase in molecular complexity.
- On the other side, we also found an increase in mobility for **G1A** and **G2A** with respect to the A ligand at this Cu (II) concentration. This is probably due to a weakness of the binding between the ions and the dendrimer sites. It seems that the ions cannot easily coordinate the nitrogen sites in the same dendrimer and work as bridges among different dendrimer molecules. Indeed, we see an opalescence in the solution which indicates a phase separation.
- On this basis, the intensity of the spectra of **G3A** is very low and therefore a large fraction of ions gives rise to a precipitate and the remaining fraction is providing EPR-visible complexation with ions trapped into the external dendrimer branches.
- **G1C** and **G2C** dendrimers also show to form more mobile complexes if compared to the C ligand due to the hindering played by the dendrimer branches. Only **G3C**-Cu (II) complex shows a slower mobility with respect to the C ligand - Cu (II) complex, but the mobility is faster that that measured for **G3A** and **G3B** complexes.
- The B series shows a different behavior because the B ligand is by itself more flexible and the attachment to the dendrimer backbone does not impede to the B functions to approach the ions and to form stable and less moving structures in a larger range of Cu (II) concentrations.

Figures 3(D), 3(E) and 3(F) are the same as 3(A), 3(B) and 3(C), but with a Cu^{2+} concentration of 0.1 M. The comparison between the two series of figures for Cu^{2+} at 0.05 and 0.1 M underlines the significant structural and coordination variations occurring when the ligand/Cu (II) molar ratio decreases from 2 to 1. For instance we noted that the A and C ligands are more affected by the increase in Cu (II) concentration than the B ligand and the same holds for the B dendrimers, mainly for **G3B** which shows a more homogeneous distribution of ions interacting with the dendrimer external branches in a less hindered situation. Indeed, for the mobility too, we see a decrease in τ (increase in mobility) for all systems, with the exception of **G3A**, which still shows slow mobility of the Cu-dendrimer complex, but only for a 50 % of the ions. We have again to underline the low intensity of the **G3A** spectra. This means that the external branches of this dendrimer work as a net where the ions remains trapped inside and occupy close sites undergoing to strong spin-spin interactions with a consequent decrease in intensity. However, 50 % of the ions cannot enter the net and are confined outside the dendrimer.

The variation in relative percentage of the Cu-solvent complex in the spectra for Cu^{2+} at concentration 0.1 M is better resumed in Figure 3(G). This provides a measure of the saturation conditions of the ligand and dendrimers complexation ability at this Cu concentration. The analysis of this histogram further demonstrates the above findings, as such as, the lower saturation of B and **G3C** dendrimers. Conversely, the ions easily saturated the nitrogen ligands in the A series. However, the highest generations always show a higher availability of the nitrogen sites for Cu (II) complexation.

Figure 3: Comparison of different parameters obtained from computation of the EPR spectra and components, for the different systems (ligands and dendrimers): g_{xx} at $[Cu^{2+}]$ = 0.05 M (A); A_{zz} at $[Cu^{2+}]$ = 0.05 M (B); τ at $[Cu^{2+}]$ = 0.05 M (C); g_{xx} at $[Cu^{2+}]$ = 0.1 M (D); A_{zz} at $[Cu^{2+}]$ = 0.1 M (E); τ at $[Cu^{2+}]$ = 0.05 M (F); and % of Cu-solvent component at $[Cu^{2+}]$ = 0.1 M (G). For the spectra containing both the Cu-solvent and the Cu-NxOy components, only the parameters of the latter component are reported in the figures, also indicating the percentage of this component. The accuracy is ±0.001 for g_{xx}, ± 0.5 G for A_{zz}, ± 0.01 ns for τ, and ± 2 % for the percentage.

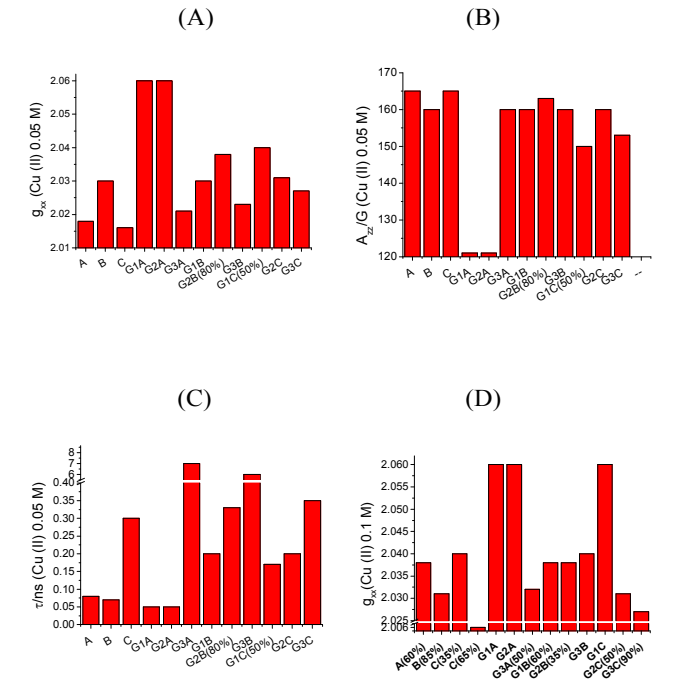

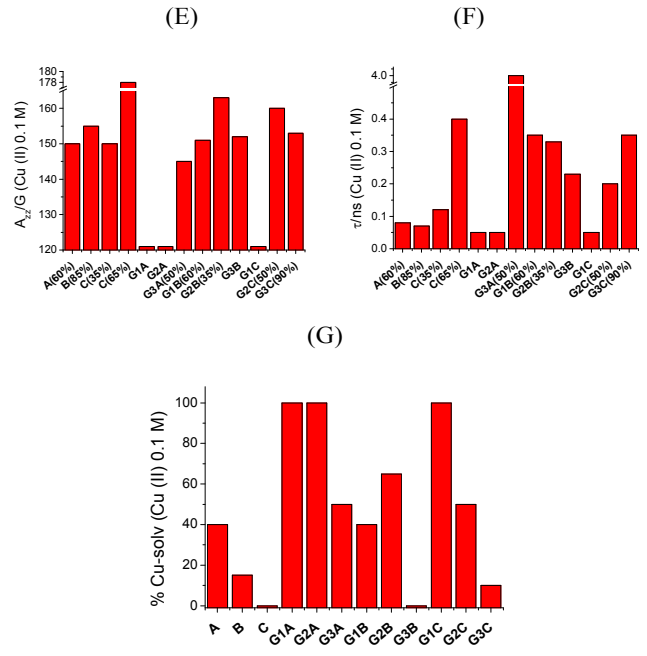

The absolute intensity of the spectra is not reported in Table 1 since it is not an accurate parameter, but, from the spectra in Figure 2, we clearly see that some spectra are more noisy than others, even if all the spectra were recorded in the same experimental conditions. On the basis of this simple visual comparison, we noted interesting behaviors in respect to the variation of the absolute intensity of the EPR spectra, which may be nicely correlated with the information extracted from Table 1, as follows:

For the A series, at the lowest Cu concentrations (0.01 M concentration may be used for a matter of comparison), the monomer A and **G1A** provide a very low intensity signal (see ESI, Figure S1), while **G2A** and **G3A** gave intensities similar to the blanks (Cu (II) in water solution). These results indicate that the monomer and the smallest dendrimer form aggregates around the ions which in part precipitate from the solution. This means that the ions work as bridges between the monomer and small dendrimer molecules using the external nitrogen groups. For **G2A** and **G3A**, the spectrum intensity is recovered and, as indicated in Table 1, the ions coordinate nitrogen and oxygen sites in a quite slow moving conditions.

This means that, in these cases, the dendrimer flexibility allows the branches of the same dendrimer molecule to approach and coordinate (chelate) the ions. For **G3A**, the more crowded external branches well justify a less-nitrogen-rich coordination and a lower mobility (CuN_3O-CuN_2O_2, and τ = 7 ns) with respect to **G2A** (CuN4, and τ = 3.3 ns) on the basis of spectral computation.

By increasing Cu(II) concentration the A monomer shows both a progressive increase in intensity and a progressive variation in Cu(II) coordination: from CuN4 between 0.01 and 0.05 M, to CuN3O between 0.05 M and 0.07 M, and to CuN2O2 between 0.07 and 0.1 M. However, CuN2O2 coexists with the Cu-solvent coordination in the spectra, and, already at 0.1 M, 40 % of the ions are only coordinating with the solvent and then the relative amount of CuN_2O_2 slowly decreases, still contributing (about 7 %) at Cu concentration of 0.5 M. The dendrimers behave in a significantly different way: **G1A** does not show any EPR signal up to 0.1 M of Cu (II), when the Cu-solvent spectrum starts contributing. So, the aggregation promoted by Cu (II) onto **G1A** works up to the 1:1 ratio between the Cu^{2+} ions and the external dendrimer groups. After the interacting sites are saturated in a bridging mode, giving rise to phase separation, at the 1:1 ratio, the extra ions are confined outside the dendrimers in solution. However **G2A** is even more easily "saturated" by Cu (II) than **G1A**, because the CuN4 coordination prevails up to 0.025 M and already at 0.03 M of Cu(II), 85 % of the "EPR visible" ions are in solution, not coordinating with the dendrimers. This is nicely explained considering that the CuN4 coordination engages 4 external nitrogen sites into the same dendrimer. But, the rigid structure of ligand A does not allow formation of a chelate complex. So, 2 neighboring external groups cannot be used in the complexation. In line with this explanation and the easy saturation of the dendrimer, the intensity variation for **G2A** spectra by increasing Cu (II) concentration is very similar to the blank. Conversely, the **G3A** dendrimer, when compared to **G2A**, provides a lower nitrogen coordination at the lowest Cu concentrations, but an enhanced coordination at a concentration of 0.1 M. So, as also described above on the basis of the histograms, the barrier played by the crowded external groups at the **G3A** surface also works as a net, where the ions may refuge and coordinate the available sites. The intensity is still very low up to 0.1 M of Cu (II), due to the spin-spin interactions occurring between close ions, sitting in neighboring interacting sites. The strong spin exchange leads to the disappearance of the EPR signal.

If we expected the B series to be similar to the A one, again, we were deluded. If compared to the A series, the B one not only gave a higher intensity of the spectra, which indicates an improved solubility of the ions, but also a more persistent coordination mainly with CuN3O-CuN2O2 configurations in a relatively faster mobility condition. Therefore the structure of these B dendrimers is more flexible at the external groups with respect to the A ones and this favors the coordination. The flexibility also avoids spin-spin interactions and enhances the Cu (II) availability to coordinate at close sites of the dendrimer surface. However, similarly to the A dendrimers, also for the B ones, G2 structure favors a CuN4 distorted coordination, while G3 better promotes a less-nitrogen-rich coordination, but, for **G3B**, stable CuN2O2 complexes are formed until Cu (II) concentration as high as 0.3 M and the spectral intensity is the highest with respect to the other systems (less noisy spectrum in Figure 2). This behavior is very peculiar for this dendrimer, and well justifies the evidence that **G3B** has a better antitumoral activity compared to **G2B** but also compared to the A and C dendrimer series. We sketched in Figure 4 the main proposed coordination modes of Cu (II) in **G3B**.

Finally, we analyzed the C series. The monomer C is significantly different in structure if compared to A and B (Figure 1), and therefore we expected a different complexation behavior with Cu (II). For the intensity, we noted an improved Cu solubility in C solutions at the lowest Cu concentrations, if compared to A and B, while the situation was inverted at the higher concentrations (from 0.1 M). The enhanced solubility in C solutions up to 0.05 M of Cu (II) is accompanied by the formation of CuN4 (distorted) coordination, where the ions form chelate complexes with two C monomers in a distorted square-planar geometry. Then, a radical change occurs at 0.1 M of Cu (II): 65 % of the ions still coordinate two monomers, but in a less distorted geometry, while the remaining 35 % only coordinates one monomer, forming a CuN2O2 coordination. In all these complexes the mobility is still in "fast motion" conditions, but much slower than found with monomers A and B, in agreement not only with the bigger size of C with respect to A and B, but also with a stronger binding between Cu and the complexing sites of C. Then, at the higher Cu concentrations, the C and A monomers behave similarly, showing a progressive decrease of a CuN2O2 coordination in favor of the Cu-solvent complexation. The B monomer show the higher percentages of nitrogen coordination at 0.1 M of Cu (II), but in much more mobile conditions and at higher absolute intensity, in line with the formation of stable complexes.

G1C shows a similar CuN4 (distorted)-CuN3O coordination as the monomer C at the lowest Cu concentrations (0.01 M), with the significant difference of the slowing down of mobility. In this case it seems that the ions are able to form a chelate complex into the same dendrimer molecule. Interestingly, by increasing Cu concentration, the intensity does not change up to 0.05 M and, already at 0.03 M of Cu (II), a slow moving CuN2O2 coordination is formed, completely substituting the CuN4 (distorted) one. Therefore the ions go to coordinate close sites, due to strong interactions with the ligands, and the strong spin-spin interactions significantly decrease the spectral intensity. The only visible interactions at 0.03 M are those involving one dendrimer branch which, due to its flexibility, may take the ions and secure them far away from the spin-spin interacting bis-chelate complexes. Saturation of these binding sites at Cu concentrations of 0.1 M leads to ions confined outside the dendrimer only complexed by the solvent.

G2C at the lowest Cu(II) concentrations coordinates less nitrogen external sites with respect to **G1C**, but, then, at higher Cu(II) concentration, CuN3O-CuN2O2 coordination are retained up to a Cu(II) concentrations of 0.1 M (1:1 between copper ions and external dendrimer surface sites).

For **G3C**, the more crowded external branches impeded the entrance of the ions at the lowest Cu(II) concentrations and the formation of stable bis-chelate complexes. Interestingly, at 0.1 M of Cu a good fraction of intensity was recovered and a CuN2O2 coordination appeared and only contributed to the spectrum, with relatively fast mobility conditions indicative of complex formation at the external surface. However, these coordination sites also saturated and at 0.3 M of Cu(II) the spectrum was characteristic of the Cu-solvent complexation.

Figure 4: Main proposed structures of the dendrimer **G3B** complexed with Cu(II).

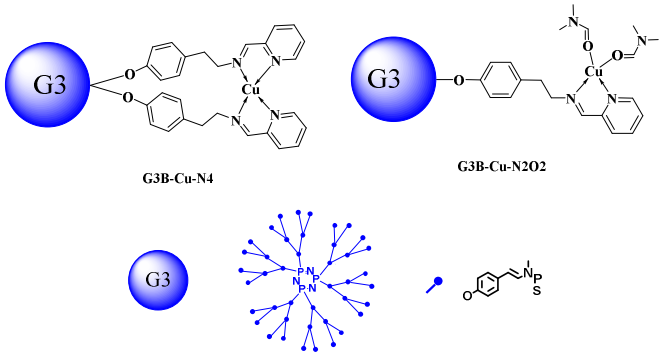

Cu (II)-dendrimers and monomers in the presence of cells

The analysis described above and the reported biological properties of the Cu (II) – **G3B** complexes[7] showed us that **G3B** dendrimer is the best candidate to study the Cu (II) complexation behavior in the presence of the cells. We also selected, on the basis of the results described above, the Cu (II) concentration of 0.05 M, which corresponds to a molar ratio between the external dendrimer functionalities and the Cu (II) ions = 2. This concentration guaranties the coordination with surface external groups of the dendrimer mostly in a CuN2O2 coordination without getting saturation of the coordination sites.

The first problem to face by using the cells is the need of a medium to guarantee cell stability. The MRC-5 (henceforth simply termed MRC) cells were dissolved in DMEM, while the tumoral cell lines HCT-116 (henceforth simply termed HCT) were dissolved in RPMI. This variation of the solvent with respect to the analysis performed for the Cu-dendrimers dissolved in DMF needed to first perform a series of controls, that is, analyze the Cu(II) solutions in DMEM and RPMI at 0.05 M, then, also analyze the same solutions after addition of the cells (without **G3B**) and after addition of **G3B** (without the cells). Finally, the complete three component systems (Cu (II) + cells + **G3B**) in the medium (DMEM for MRC cells, and RPMI for HCT cells) were analyzed. The samples in the presence of the cells were incubated for different times starting from one day to three days. Before all EPR experiments, cell viability was evaluated by Trypan blue exclusion tests and we performed the EPR study after verifying the accordance between the cell-survival percentages obtained in this study and in the study performed in ref. 7.. However, the cell death cannot be ruled out by EPR, but, as described in the following, the variation of EPR spectral features provides information about the different interacting sites and cell proliferation.

Figure 5 shows the experimental EPR spectra at 298 K for the different systems described above. Two arrows indicate the main features of two components contributing to most of the spectra.

Figure 5: Experimental EPR spectra (298 K) of Cu (II) (0.05 M) in DMEM solutions in the absence and presence of **G3B** (0.1 M in external surface groups),

MRC, and MRC+**G3B** or in RPMI solutions in the absence and presence of **G3B**, HCT, and HCT+**G3B**. The spectra of Cu (II) in DMEM and RPMI solutions are equivalent both in absence and in presence of **G3B**. The spectra were recorded after 24 h of equilibration.

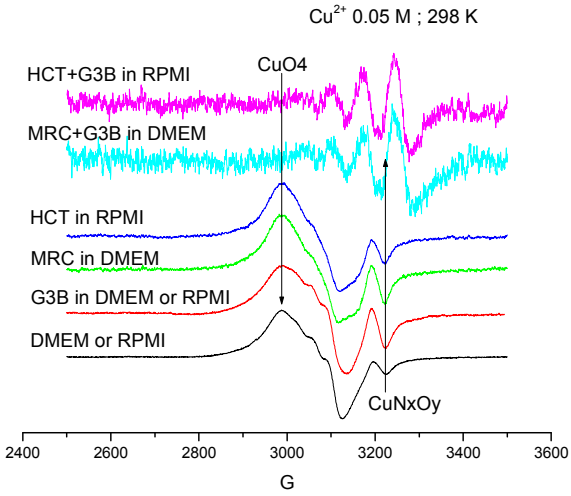

To extract and simulate the components and characterize the coordination modes of Cu (II) in these systems, we performed a subtraction procedure between the experimental spectra, both at 298 and 150 K. Figure S2 in the SI shows the computations of the extracted components, whose main computation parameters (g_{ii}, A_{zz} and τ; meaning described in the Experimental Section) are reported in Table 2.

Table 2: Main parameters (g_{ii}, A_{zz} and τ; meaning described in the Experimental Section) extracted from computation of the spectra (both at 298 and 150 K) of Cu (II) (0.05 M) in DMEM solutions in the absence and presence of **G3B** (0.1 M in external surface groups), MRC, and MRC+**G3B** or in RPMI solutions in the absence and presence of **G3B**, HCT, and HCT+**G3B**. The different coordinations, listed in the last column of the Table and obtained as described in the Experimental Section, indicated how many oxygen (O) and/or nitrogen (N) ligand sites were coordinating Cu^{2+} ions in a square planar geometry. The accuracy is ±0.001 for g_{ii}, ± 0.5 G for A_{zz}, ± 0.01 ns for τ, and ± 2 % for the percentage.

Sample	%	g_{xx}	g_{yy}	g_{zz}	A_{zz} /G	τ /ns	Coord.
no	10	2.043	2.06	2.34	140	0.02	CuO3N
--	90	2.061	2.077	2.402	119	0.05	CuO4
G3B	35	2.04	2.05	2.29	160	0.33	CuN3O-CuN2O2
--	65	2.061	2.077	2.402	119	0.05	CuO4
MRC	32	2.04	2.05	2.313	155	0.07	CuN2O2
--	68	2.061	2.075	2.399	116	0.05	CuO4
HCT	20	2.04	2.05	2.313	155	0.07	CuN2O2
--	80	2.061	2.075	2.399	116	0.05	CuO4
MRC+G3B	100	2.014	2.033	2.227	189	0.07	CuN4
HCT+G3B	100	2.014	2.033	2.229	185	0.05	CuN4

From the analysis of the spectra in Figure 5 and the parameters in Table 2, we extract the following information:

- If compared with Cu (II) in DMF solutions, the spectrum of Cu (II) in DMEM or RPMI solutions (without cells and dendrimer) also contains a 10 % of a nitrogen coordinated component, which, on the basis of the magnetic parameters, was correlated with a CuO3N coordination. This means that the media solutions contain a fraction of nitrogen ligands, which may interfere with the coordination of Cu (II) with other nitrogen ligands belonging to the dendrimer and the cells. The mobility of the ions involved in the CuO_3N coordination in the media is very fast. However, the most of Cu (II) (90 %) in the media coordinates oxygen ligands from the medium itself (CuO4). The spectrum is almost equivalent to the one found for Cu (II) in DMF solutions, but with a stronger coordination between Cu (II) and the oxygen-sites of the growth medium as tested by the lower A_{zz} in the latter case.
- In the binary system obtained by adding **G3B** to the Cu (II) solutions in DMEM and RPMI (without the cells) we did not find the same situation as described above for Cu (II) + **G3B** in DMF solutions. In DMF solution all Cu (II) was complexed at the dendrimer surface, while, in DMEM or RPMI, only 35 % of Cu(II) is involved in a CuN_3O-CuN_2O_2 coordination with the dendrimer external functions, while the remaining 65 % are extruded from the dendrimer, forming the CuO_4 coordination found in the pure media solutions (without **G3B**, as at point 1.). This means that the media (DMEM and RPMI) contain components (probably the metal ions) which interact with the nitrogen sites of B in **G3B** inducing an earlier saturation of these sites in coordination with Cu (II).
- The binary systems formed by Cu (II) in the cell culture dispersions (in the absence of the dendrimers) show an interesting behavior. Apparently the spectra for the two binary systems, Cu (II) + **G3B** and Cu (II) + cells, in Figure 5 are quite similar to each other but the data in Table 2 show a different story. First, the main parameters (Table 2) of the two components constituting the spectra change from Cu (II) + **G3B** to Cu (II) + cells. This change indicates that the CuN_3O-CuN_2O_2 component in Cu (II) + **G3B** transforms into a CuN_2O_2 component in Cu (II) + cells, that is, less rich in nitrogen sites. This component is also more mobile for Cu (II) + cells if compared with Cu (II) + **G3B**. This indicates a new and more fluid environment for the ions interacting with the cells with respect to the ions interacting with the dendrimers. However, we also noted quite different magnetic parameters for the CuO4 component in the case of Cu (II) + cells, compared to the ions in pure media solutions or in the media containing **G3B**: A_{zz} diminished, while g_{zz} increased. This behavior is usually found for an increasing strength in the Cu-oxygen site coordination. Therefore, this henceforth termed new-CuO4 coordination in the binary system Cu (II) + cells is ascribed to ions interacting with oxygen sites belonging to the cells. It is also evident a variation of the relative percentages of the components: the new-CuO4 coordination is at higher percentage with respect to the "old" one for the Cu (II) + **G3B** system, but it is still at lower percentage with respect to the old-CuO4

for Cu (II) alone in the media However, what is in our opinion more important is that the relative percentages of the CuN2O2 and the new-CuO4 components change from MRC to HCT solutions, that is, 32 % of the CuN_2O_2 component for the MRC solutions and 20 % for HCT solutions. Therefore Cu (II) in the cancer cells (HCT) shows a preferred interactions with the oxygen sites in the cell structure if compared to the healthy cells (MRC), but the interacting sites seem equivalent for the two cell lines.

- For the ternary systems (Cu (II) + **G3B** + cells) in the media solutions we first tried to understand if the sequence of addition of the three ingredients was relevant. We found that a variable (over time and mixing conditions) fraction of ions retained the spectrum of Cu (II) + **G3B** if the cells were added at the end, and, similarly, a variable (over time and mixing conditions) fraction of ions retained the spectrum of Cu (II) + cells if the dendrimer was added at the end. Conversely, the spectra were well reproducible over time and mixing conditions and provided interesting information if the ions were added after mixing the cells and **G3B** in the media solutions. Indeed the spectra completely changed with respect to the binary systems and they were constituted by a single component characteristic of a CuN4 coordination. Therefore, the binding between the dendrimer and the cells offers more nitrogen interacting sites available to the ions with respect to dendrimers and cells alone. We think that the dendrimer-cell interaction uses the oxygen sites, but also modifies the structure of the dendrimer favoring the coordination of Cu (II) with 4 nitrogen sites in a fluid condition (fast mobility). Furthermore, the spectra become much less intense. This means that the oxygen sites are engaged in forming self - aggregated structures where the Cu (II) ions are concentrated or separate from the solution and therefore they disappear from the spectra. On the other side, the CuN4 coordination becomes more probable because in self-aggregated (supramolecular) structures more nitrogen sites are available in the same space region, able to host the Cu (II) ions. However, these nitrogen sites belong to the external branches of the supramolecular structure and retain a high flexibility which well justifies the high rotational mobility of the complexed ions.
- Finally we see some interesting differences between the Cu (II) + MRC + **G3B** and the Cu (II) + HCT + **G3B** spectra. Mainly, we noted that the spectrum of Cu (II) + MRC + **G3B** is at much lower intensity (much more noisy, in Figure 5) with respect to the spectrum of Cu (II) + HCT + **G3B**. This indicates a higher stability of the latter system, while Cu (II) in the MRC + **G3B** system is concentrating in confined space leading to strong spin-spin interactions which in turn lead to an intensity decrease. In line with this, the binding between Cu (II) (quite few remaining "EPR-alive" for the MRC samples) and the nitrogen sites is a little bit stronger and the mobility a little bit slower in the MRC-containing sample with respect to the HCT case, since the ions are forced to come closer to the nitrogen sites at the **G3B**-MRC/solution interphase. These findings are in line with previous results[7] which indicate a stronger binding of Cu-**G3B** with HCT cells with respect to the MRC ones.
- Further information came from the effect of different equilibration times in the cell containing samples. The spectra shown in Figure 5 were obtained after 24 hours of equilibration time. The spectrum of the ternary system containing HCT was invariant for the line shape over time, but the intensity increased a little bit from 24 to 48 h, while it decreased of about 20 % after 72 h. This decrease in intensity may be related to the production of radicals which usually accompanies the growth of cancer cell and well agrees with the measure of the inhibition of cell proliferation of about 80 %.[7] Conversely, the spectrum with MCR showed a small decrease in intensity from 24 to 48 hours of equilibration but then, from 48 h to 72 h the overall intensity increased but the CuO4 component also appeared indicating that the ions are partly detached from the binding sites coming back to the oxygen cell sites. As shown in ref. 7, MCR cells complexed by Cu (II) show an unexpected increase in IC_{50}. Therefore, the behavior over time for the cancer cells and the difference between cancer and healthy cells are nicely related to the effect of the dendrimer-Cu (II) complex on the cell proliferation.[7] In Figure 6, the values of IC_{50} for the two cell lines from ref. 7 are compared to the variations in intensity of the EPR signal (expressed as intensity ratio), showing the good agreement between these measurements. This agreement demonstrates that EPR analysis not only provides information about interactions and dynamics at molecular level, but also supports and rationalizes some biological data.

Figure 6: IC_{50} for the two cell lines from ref. 7 compared to the variations in intensity of the EPR signal (expressed as intensity ratios)

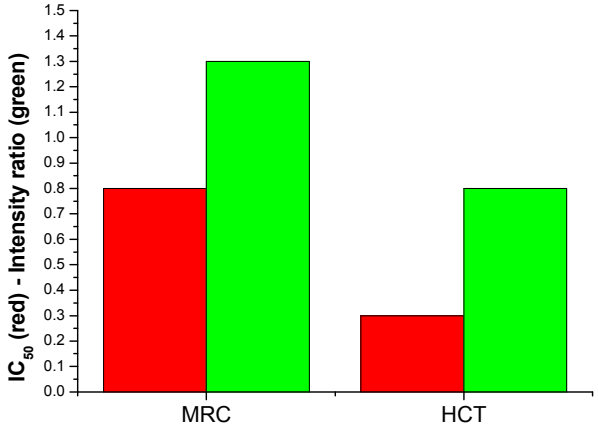

Definitely, the EPR analysis demonstrated to be useful to clarify the interaction modes of Cu (II) ions in biologically relevant systems like those containing health and cancer cells and dendrimers able to interact with the cells in a more specific binding behavior, which is driven by Cu (II) ions.

Experimental

Materials and Sample Preparation.

The dendrimers were synthesized as reported in ref. 7. The dendrimers were dissolved in DMF resulting in a final external surface group concentration of 0.1 M. For a correct comparison, solutions of the A, B, and C molecules were prepared at the same concentration. Cupric nitrate hydrate (Cu $(NO_3)_2$ $2.5H_2O$, Sigma- Aldrich, ACS reagent 98 %) was also dissolved in DMF and mixed with the solutions of dendrimers and A, B, and C, to obtain a final concentration of Cu^{2+} from 0.0025 M to 0.5 M. After different equilibration times (from freshly prepared to one day aging), 100 µL of the dendrimer (or A, B, C)-copper solutions were inserted in an EPR tube (1 mm internal diameter). We verified that the equilibration time did not affect the EPR result.

Normal human fetal lung fibroblast cells, MCR-5, were grown in DMEM supplemented with 10% fetal calf serum (FCS) in a 5% CO_2 atmosphere at 37 °C. Before incubation, culture medium was removed and MCR-5 were resuspended in Trypsin (2/3 ml per T25 cell culture flask); the cells were maintained at 37° C with 5% CO_2 for 3 min., then, MCR-5 cells were centrifuged (1200 rpm) for 10 min, and cell viability was evaluated by Trypan Blue exclusion tests. Cells were divided in 96 wells (2000 cells per 100 µl) and were incubated for 48 h and 72 h with $Cu(NO_3)_2$ hydrate and in the absence and presence of **G3B**.

Human colon carcinoma cell line, HCT-116, were grown in RPMI 1640 supplemented with 10 % FBS in a 5% CO_2 atmosphere at 37 °C. Before incubation, culture medium was removed, and HTC-116 cells were resuspended in Trypsin (2/3 ml per T25 cell culture flask) and were maintained at 37° C with 5% CO_2 for 3 min. Then, HTC-116 cells were centrifuged (1200 rpm) for 10 min, and cell viability was evaluated by Trypan Blue exclusion tests. Cells were divided in 96 wells (2000 cells per 100 µl) and were incubated for 48 h and 72 h with $Cu(NO_3)_2$ hydrate and in the absence and presence of **G3B**. These samples were inserted in the EPR tubes for the analysis.

Methods.

EPR spectra were recorded by means of an EMX-Bruker spectrometer operating at X band (9.5 GHz) and interfaced with a PC (software from Bruker for handling and analysis of the EPR spectra). The temperature was controlled with a Bruker ST3000 variable-temperature assembly cooled with liquid nitrogen. The EPR spectra were recorded for the different samples at 298K and 150 K.

In all cases, we controlled the reproducibility of the results by repeating the EPR analysis (three times) in the same experimental conditions for each sample.

All the spectra were performed in the same instrumental conditions to permit a comparison for the absolute intensity among the different samples. In these conditions, termed "standard" (receiver gain $6.32x10^2$, modulation amplitude 3 G, time constant 10.24 msec, conversion time 40.96 msec, resolution 2048 points, number of scans 10, EPR tube size 2 mm internal, liquid volume 50 □L, temperature 298 and 150 K), all the "blank" spectra (Cu in the solvent) are well visible. Of course we repeated the EPR measurement by increasing the number of scans when the spectra are no more visible at the "standard" conditions, meaning that only a fraction of ions contribute to the spectra.

Computation of the EPR spectra and identification of Cu (II)-coordination sites and structures.

The low temperature EPR spectra were computed by first comparing different methods, as such as the CU23 program kindly provided by Prof. Romanelli, University of Florence, Italy; the Bruker's WIN-EPR SimFonia Software Version 1.25; the method reported by Bennett *et al.*,[14, 15] the program EasySpin 4.5.1, using MATLAB 7.5; and the procedure by Budil *et al.* for computing nitroxide radical spectra.[16] This last procedure was successfully applied to the computation of Cu (II) spectra at both room and low temperature. In this latter case the computation also provides information about the mobility of the Cu-complex, which is related to the flexibility of the dendrimer structure in the region where Cu^{2+} is located. Therefore, the main parameters used for the computation of the spectra at both low and room temperatures were: (a) the g_{ii} components (accuracy in the third decimal, on the basis of the computation itself) for the coupling between the electron spin and the magnetic field; (b) the A_{ii} components (accuracy of about ± 0.5 G) for the coupling between the electron spin and the copper nuclear spin (I_{Cu} = 3/2); (c) the correlation time for the diffusion rotational motion of the complexed Cu (II) ions, □, and (d) the line widths W_{ii} of the x, y, and z lines. The magnetic parameters, g_{ii} and A_{ii} were first directly measured in the low temperature spectra by field calibration with the DPPH radical (g = 2.0036), and then we verified the accuracy of the computation by using the different procedures described above to get the best fitting between the experimental and the computed spectra.

In several cases the spectra were constituted by two or three components due to different coordination and geometries of Cu (II)-dendrimer complexes. The subtraction between the spectra in different experimental conditions allowed extraction of the spectral components constituting the overall EPR spectra. The different components were computed separately. The subtraction procedure also allowed us to calculate, by double integration of each component, the relative percentages of the different components, with an accuracy of 2 %.

We found that the simulations of the observed EPR signals provided a useful means of estimating the spectral parameters but did not necessarily produce unique fits. However, we trusted the parameters which provided best fitting of a series of spectra in similar experimental conditions.

The magnetic parameters extracted from the computation were then compared with equivalent parameters found in the literature.[8-13,17-35] This allowed us to assign each spectral

component to a copper coordination and identify the structure and complexing sites of the dendrimers.

We first noted that the magnetic parameters (g_{ii} and A_{ii}) were characteristic of a square planar coordination (axially elongated octahedral), eventually tetrahedrally distorted, for all the systems, with the d_{x2-y2} orbital as ground state.

Conclusions

The increasing widespread use of monomeric copper complexes as anticancer agents is mainly due to their possibilities to overcome some drawbacks encountered when, for example, more classical metallodrugs as cisplatin are employed. This finding and, more, our promising preliminary results concerning the antitumoral effects of copper conjugated phosphorus dendrimers prompted us to investigate the complexation mode of these phosphorus dendrimers of different generation incorporating diverse ligands able to complex Cu (II) on their surface. The accurate EPR analysis showed subtle changes on the coordination mode, on the mobility and on the stability of the resulting Cu (II) complexes when increasing the concentration of Cu (II). The different coordination modes such as CuN4, CuN3O, CuN2O2, and CuNO3, mainly depended on the nature of the ligands decorating the external shell of the dendrimers and the generation of the dendrimer. After saturating the external ligands coordination ability, the ions were confined externally in CuO4 coordination with the solvent. These studies clearly demonstrate that, among all the dendrimer complexes, the Cu (II) complex with the so-called **G3B** dendrimer showing a CuN2O2 coordination appears to be the most stable.

A detailed investigation concerning Cu (II)-**G3B** complex in the presence of two types of cells, human fetal lung fibroblast cells, MCR-5, and human colon carcinoma cell line, HCT-116, were performed, allowing to point out some significant change in the coordination mode as well as a higher stability of the Cu–HCT-**G3B** complex thus corroborating our previous observation concerning the anti-tumoral properties and selectivity of this Cu(II) dendrimer complex. Elucidation of the mechanism of action of **G3B**-Cu in the cells is underway.

Acknowledgements

MFO acknowledges financial support from PRIN2012 – NANOMed. COST Actions MP1202 and TD0802 are also acknowledged for supporting networking.

Notes and references

[a] Department of Earth, Life and Environment Sciences, Località Crocicchia, University of Urbino, 61029 Urbino, Italy : maria.ottaviani@uniurb.it; michela.cangiotti@uniurb.it; concetta.coppola@uniurb.it; flavia.buccella@uniurb.it;
[b] CNRS, LCC (Laboratoire de Chimie de Coordination), 205 route de Narbonne, BP44099, F-31077 Toulouse Cedex 4, France : nabil.elbrahmi@lcc-toulouse.fr; anne-marie.caminade@lcc-toulouse.fr; costes@lcc-toulouse.fr; majoral@lcc-toulouse.fr
[c] Euro-Mediterranean University of Fez, Fès-Shore, Route de Sidi harazem, Fès, Morocco
[d] ICSN-CNRS UPR 2301, Avenue de la Terrasse, 91198 Gif sur Yvette, France : thierry.cresteil@cnrs.fr
[e] Laboratoire de Chimie et de Biochimie Pharmacologiques et Toxicologique, Université Paris Descartes, PRES Sorbonne Paris Cité, CNRS UMR 860, 45, rue des Saints Pères, Paris 75006, France : serge_mignani@orange.fr

* corresponding authors : maria.ottaviani@uniurb.it ; majoral@lcc-toulouse.fr

Electronic Supplementary Information (ESI) available: Examples of experimental and computed EPR spectra. See DOI: 10.1039/b000000x/

1) a) J. Khandare, M. Calderon, N. M. Dagia, and R. Haag, *Chem. Soc. Rev*., 2012, **41**, 2824-2848; b) S. H. Medina, and M. E. H. El-Sayed, *Chem. Rev.,* 2009, **109**, 3141-3157; c) R.K Tekade, P. V. Kumar, and N. K. Jain, *Chem.Rev*. 2009, **109**, 49-87; d) R. Duncan, and L. Izzo, *Adv.Drug Delivery Rev.,* 2005, **57**, 2215-2237 ; e) U. Boas, and P. M. H. Heegaard, *Chem. Soc. Rev*., 2004, **33**, 43-63.

2) a) S. Mignani, S. El Kazzouli, M. Bousmina, and J. P. Majoral, *Chem. Rev.,*2014, **114**, 1327-1342**;** b) S. Mignani, S. El Kazzouli, M. Bousmina, and J. P. Majoral *Progress in Polymer Science,* 2013, **38**, 993-1008; c) S. Mignani, S. El Kazzouli, M. Bousmina, and J.P. Majoral, *Adv. Drug Delivery Rev.***,** 2013, **65**, 1316-1330; d) S. Mignani, and J.P Majoral, *New. J. Chem***.** 2013, **37**, 3337-3357

3) See for example: a) A.M. Caminade, and J.P. Majoral, *New J. Chem*. 2013, **37**, 3358-3373; b) J. Lazniewska, K. Milowska, M. Zablocka, S. Mignani, A.M. Caminade, J.P. Majoral, M. Bryszewska, and T. Gabryelak, *Mol. Pharmaceutics*, 2013, **10**, 3484-3496; c) K. Milowska, J. Grochowina, N. Katir, A. El Kadib, J. P. Majoral, M. Bryszewska, and T. Gabryelak, *Mol. Pharmaceutics*, 2013, **10**, 1131-1137; d) M. Hayder, M. Poupot, M. Baron, D. Nigon, C.O. Turrin, A. M. Caminade, J. P. Majoral, R. A. Eisenberg, J. J. Fournie, and A. Cantagrel, *Science Translational Medicine* 2011, **3,** 81ra35; e) L. Griffe, M. Poupot, P. Marchand, A. Maraval C.O. Turrin , O. Rolland, P. Métivier, G. Bacquet, J. J. Fournié, A. M. Caminade, R. Poupot, and J.P. Majoral, *Angew. Chem. Int. Ed.* 2007, **46**, 2523-2526; f) A. V.Maksimenko, V.Mandrouguine ,M. B. Gottikh, J. R. Bertrand, J. P. Majoral, and C. Malvy, *J. Gene Med.*, 2003, **5**, 61-71.

4) S. El Kazzouli, N. El Brahmi, S. Mignani, M. Bousmina, and J. P. Majoral, *Current Med. Chem*., 2012, **19**, 4995-5010.

5) C. Santini, M. Pellei, V. Gandin, M. Porchia, F. Tisato, and C. Marzano, *Chem. Rev*., 2014, **114**, 815-862

6) X. Zhao, S. C. J. Loo, P. P. Lee, T. T.Y. Tan, and C. K. Chu., *J. Inorg. Biochem*., 2010, **104**, 105-110.

7) N. El Brahmi, S. El Kazzouli, S. Mignani, E. M. Essassi, G. Aubert, R. Laurent, A. M. Caminade, M. Bousmina, and J. P. Majoral, *Mol. Pharmaceutics*, 2013, **10**, 1459-1464.

8) M. F. Ottaviani, S. Bossmann, N. J. Turro, and D. A. Tomalia, *J. Am. Chem. Soc.*, 1997, **116**, 661-671.

9) M. F. Ottaviani, F. Montalti, N. J. Turro, and D. A. J. Tomalia*, Phys. Chem. B,* 1997, **101**, 158-166.

10) M. F. Ottaviani, R. Valluzzi, and L. Balogh, *Macromolecules,* 2002, **35**, 5105-5115.

11) D. Appelhans, U. Oertel, R. Mazzeo, H. Komber, J. Hoffmann, S. Weidner, B. Brutschy, B. Voit, and M.F. Ottaviani, *Proc. R. Soc. A* 2010, **466,** 1489-1513.

12) M.F. Ottaviani, M. Cangiotti, A. Fattori, C. Coppola, S. Lucchi, M. Ficker, J. F. Petersen, and J. B. Christensen, *J. Phys. Chem. B*, 2013, **117**, 14163–14172.

13) M.F. Ottaviani, M. Cangiotti, A. Fattori, C. Coppola, P. Posocco, E. Laurini, Z. Liu, C. Liu, M. Fermeglia, L. Peng, and S. Pricl, *Phys. Chem. Chem. Phys.*, 2014, **16,** 685 – 694.

14) B. Bennett, W. E. Antholine, V. M. D'souza, G. J. Chen, L. Ustinyuk, and R.C. Holz, *J. Am. Chem. Soc.,* 2002, **124**, 13025-34.
15) D.M. Wang, and G.R. Hanson, *J. Magn. Reson. A,* 1995, **117**, 1-8.
16) D.E. Budil, S. Lee, S. Saxena, and J.H. Freed, *J. Magn. Res. A,* 1996, **120**, 155-189.
17) H. Beinert, *Coord. Chem. Rev.* 1980, **33**, 55-85.
18) G. Malmstrom, and T. Vanngard, *J. Mol. Biol.,* 1960, **2**, 118-124.
19) R. Aasa, R. Petterson, and T. Vanngard, *Nature,* 1961, **190**, 258-259.
20) R. D. Gillard, R.J. Lancashire, and P. Obrien, *Transition Met. Chem.,* 1980, **5**, 340-345.
21) H. Gampp, *Inorg. Chem.,* 1984, **23**, 1553-1557.
22) M. McBride., *Soil Sci. Soc. Am. J.* 1991, **55**, 979-985.
23) M. M. Hassanien, I. M. Gabr, M. H. Abdel-Rhman, and A. A. El-Asmy, *Spectrochim. Acta,* 2008, **71,** 73-79.
24) M. Unno, and M. Ikeda-Saito, *Adv Mater. Res.,* 2009, **13**, 193-217.
25) B. Kozlevcar, and P. Segedin, *Croatica Chem. Acta*, 2008, **81**, 369-379.
26) R. Basosi, G. Della Lunga, and R. Pogni, *Biol. Magn. Reson.,* 2005, **23**, 385-416.
27) A.C. Saladino, and S.C. Larsen, *Catalysis Today,* 2005, **105**, 122-133.
28) J. Zhang, M.J.N. Junk, J. Luo, D. Hinderberger, and X.X. Zhu, *Langmuir,* 2010, **26**, 13415-13421.
29) J. Peisach, and W.E. Blumberg, *Arch. Biochem. Biophys*., 1974, **165**, 691-708.
30) A. W. Addison, K. D. Karlin, and J. Zubieta, Eds.; Adenine Press: Guilderland, New York, 1983; p 109-115.
31) N. Wei, N. N. Murthy, and K. D. Karlin, *Inorg. Chem.,* 1994, **33**, 6093-6100 and references therein.
32) M. R. Malachowski, H. B. Huynh, L. J. Tomlinson, R. S. Kelly, and J. W. Furbee jr., *J. Chem. Soc. Dalton. Trans.* 1995, 31-36.
33) E. I. Solomon, and M. A. Hanson, *Bioinorganic Spectroscopy in Inorganic Electronic Structure and Spectroscopy, Volume II: Applications and Case Studies*; Solomon, E. I., Lever, A. B. P., Eds.; John Wiley & Sons: New York, 2006; pp 1-130.
34) B. J. Hathaway, M. Duggan, A. Murphy, J. Mullane, C. Power, A. Walsh, and B. Walsh, *Coord. Chem. Rev.,* 1981, **36**, 267-324.
35) E. Garribba, G. Micera, D. Sanna, and L. Strinna-Erre, *Inorg. Chim. Acta,* 2000, **299,** 253-261.

